LANGMUIR Article
Cite This: Langmuir 2017, 33, 13945−13954
pubs.acs.org/Langmuir

Measurement of Charge Transfer to Aqueous Droplets in High Voltage Electric Fields

Eric S. Elton, Yash Tibrewala, Ethan R. Rosenberg, Brad S. Hamlin, and William D. Ristenpart*

Department of Chemical Engineering, University of California at Davis, Davis, California 95616, United States

Supporting Information

ABSTRACT: The electric charge acquired by aqueous droplets when they contact an electrode is a crucial parameter in experimental and industrial applications where electric fields are used to manipulate droplet motion and coalescence. For unclear reasons, many investigators have found that aqueous droplets acquire significantly more positive than negative charge. Extant techniques for determining the droplet charge typically rely on a hydrodynamic force balance that depends on accurate characterization of the drag forces acting on the droplet. Here we present an alternative methodology for measuring the droplet charge via direct measurement of the electric current. As the droplet approaches the electrode the current is observed to gradually increase, followed by a large pulse when the droplet makes apparent contact. We interpret the transient current signals as the superposition of the natural response of an RLC circuit and an induced current described by the Shockley−Ramo theory. Nonlinear regression of the observed current to the theoretical model allows for the droplet charge to be extracted, independent of any assumptions about the force balance on the droplet. We demonstrate that regression of the current signal yields charge values that are on average within 4% of charges measured via a force balance. We use the chronocoulometric methodology to investigate how the charge varies with the applied potential, and we demonstrate that deionized water droplets contacting planar electrodes acquire on average 69% more positive charge than negative charge.

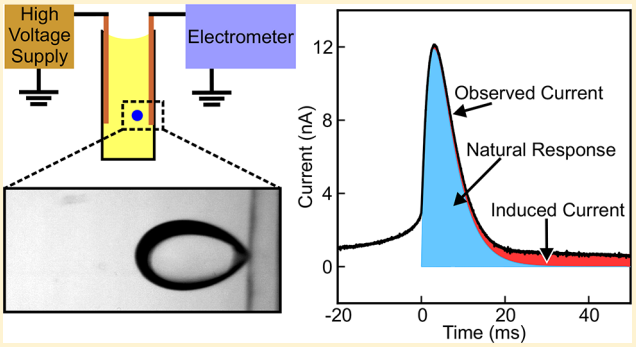

INTRODUCTION

Many important applications involve charged water droplets in oil. Industrially, electric fields have been used since the early 20th century to enhance the phase separation of water-in-oil emulsions;[1] attractive Coulombic forces between oppositely charged droplets induce them to coalesce and consequently sediment more rapidly.[2] Electric fields are also effective for controlling droplet motion and coalescence in microfluidic applications.[3−7] For instance, application of an electric field between two oppositely charged droplets can induce coalescence between them where otherwise coalescence would not occur, either at a T-junction[8] or in line with the flow channel.[9−11] A number of investigations have described the charging and motion of droplets in electric fields in the context of simulating liquid/liquid extractors,[12] droplet formation,[6,7] emulsion electric properties,[13] solute delivery for biological applications,[14] sorting and electroporation of cells,[15,16] and surface dewetting.[17]

The measurement of the charge acquired by the droplet is of fundamental interest for many applications. For example, droplets may partially coalesce, completely coalesce, or not coalesce depending on the net charge and conductivity of the droplet.[18,19] Similarly, charged droplets may break apart producing many much smaller droplets if the electric field or droplet charge exceed critical values.[20,21]

In addition, accurate measurements of the droplet charge are required to understand some basic unexplained observations. For example, a review of reports of droplets bouncing between parallel plate electrodes over the last 15 years reveals that droplets regularly acquire more positive than negative charge (see Table 1).[14,22−27] Despite this phenomenon being widely reported, no attempts have been made to explain it or provide insight into why it occurs. From an electrostatic approach, there is no clear reason why droplets should acquire different amounts of charge from different polarity electrodes; solid metal particles are not observed to have this disparity in charge.[24,28−30] Similarly, droplets are also observed to acquire varying amounts of the theoretical maximum amount of charge, as calculated by Maxwell.[31] Although the Maxwell prediction is based on a perfectly conducting spherical particle contacting a planar electrode, it is expected that water droplets would show similar behavior. Solid particles have also been shown to receive less than the theoretical amount of charge, although the reason for this is unclear.[28,32]

The measurement of charge acquired by the droplet is also of importance in understanding the fundamental charge transfer

Received: September 26, 2017
Revised: November 6, 2017
Published: November 15, 2017

ACS Publications © 2017 American Chemical Society

DOI: 10.1021/acs.langmuir.7b03375
Langmuir 2017, 33, 13945−13954

Table 1. Review of Published Reports of the Charge Acquired by Aqueous Droplets[a]

ref	insulating fluid	droplet fluid	drop diameter	electric field (kV/cm)	Q_{pos}/Q_{neg}	$Q_{pos}/Q_{Maxwell}$
14	silicone oil	0.15 M KCl	1.2 mm	5.1	1.25	0.46
22	silicone oil	DI water	1.2 mm	5.0	1.16	1.42
23	silicone oil	DI water	1.6 mm	2.0	1.24	0.88
24	silicone oil	aqueous buffer	2.0 mm	4.1	1.82	1.33
25	calibration oil	Tap water	1.0 mm	3.5	1.23	0.0017
26	transformer oil	DI water	3.0 mm	2.0	1.55	0.83
27	silicone oil	DI water	1.2 mm	2.5	2.63	0.66
this work	silicone oil	DI water	1.5 mm	4.5	1.69	0.75

[a] Q_{pos} is the average positive charge of the droplet. Q_{neg} is the average negative charge of the droplet. $Q_{Maxwell}$ is the theoretical amount of charge acquired by a conducting sphere of the same diameter as the droplet in contact with a planar electrode in the same electric field as calculated by eq 12.

mechanism. The exact mechanism of charge transfer between electrodes and water droplets is unknown, although authors have speculated that charge transfer may be due to electrochemical reactions which presumably occur during droplet contact with the electrode.[5,22,23] It has also recently been shown that dielectric breakdown, evidenced as a flash of light detected as the droplet approached the electrode, can occur between water droplets and electrodes during charge transfer events although the droplet appears to make contact with the electrode during each charge transfer event.[24] The breakdown event was observed to physically deform the electrodes, with craters and other morphologies being formed on the electrode surface. Accurate measurement of the charge acquired by the droplet is crucial to elucidating the charge transfer mechanism.

A key challenge in understanding charge transfer into water droplets is that extant techniques to measure droplet charge rely on an indirect approach. Specifically, the most common technique relies on a force balance between the electrophoretic and drag force,[5,14,18,22−27] similar to how Millikan first measured the elementary charge.[33] Typically, the flow is assumed to be inertialess, and, assuming that the droplet is moving horizontally, the force balance can be written as

$$\sum F = F_d + F_E = 0 \tag{1}$$

where $F_E = QE$ is the electrophroetic force and $F_d = 4\pi\mu a\vec{u}\lambda$ is the drag force. Here Q is the droplet charge, E is the applied electric field, a is the droplet radius, μ is the oil viscosity, $\vec{u}$ is the droplet velocity, and λ is a correction factor to account for additional drag forces in the experimental cell. The final expression for the droplet charge is then:

$$Q = \frac{4\pi\lambda\mu a\vec{u}}{\vec{E}} \tag{2}$$

Typically the parameters in eq 2 other than the droplet velocity are known a priori, so visual observation of the droplet velocity yields everything necessary to calculate the droplet charge. Modern applications of this technique typically record video of the droplet motion, so as to obtain an accurate measure of the droplet velocity.

A crucial caveat in this force balance approach, however, is the assumption that one knows λ precisely. In practice, λ is difficult to describe. A liquid sphere with a fluid interface in an infinite, quiescent medium should follow the Hadamard−Rybczynski solution,[34,35]

$$\lambda = \frac{3\hat{\mu} + 2}{2(\hat{\mu} + 1)} \tag{3}$$

where $\hat{\mu} = \frac{\mu_d}{\mu}$ is the ratio of the droplet viscosity to the oil viscosity.[36] In the limit of an inviscid droplet ($\mu_d \ll \mu$), then $\lambda \to 1$ and the drag force is $F_d = 4\pi\mu a\vec{u}$. Liquid droplets are often observed experimentally to sediment as if they are solid spheres, however, with a drag of $F_d = 6\pi\mu a\vec{u}$ ($\lambda = 1.5$).[36−38] This reduction in velocity is often due to a "stagnant cap" of surfactant molecules on the surface of the droplet which exert Marangoni stresses that impede internal recirculation.[36,39,40] In other words, using the incorrect value of λ can cause up to a 50% error in the charge calculated via eq 2.

Even if one precisely knows the surfactant concentration and the corresponding drag due to the stagnant cap, several other effects complicate matters. For example, the above expression for λ does not take into account the increased viscous hindrance due to the container walls and electrodes.[36,41] In the limit of Stokes flow, λ actually diverges as the separation between the droplet and solid surface goes to zero (i.e., $\lambda \to \infty$ as $h \to 0$). Similarly, droplets deform in electric fields and may become nonspherical, which can cause significant deviation in the drag coefficient.[21,36] Finally, the droplet must reach a constant velocity (zero acceleration) in order for eq 2 to be accurate. This condition can be hard to obtain for droplets which have similar diameters to the electrode spacing. Given these complications, a more direct approach, which does not rely on characterizing the drag force on the droplet, to determine droplet charge is desirable.

One attractive technique for determining the charge obtained by a particle contacting an electrode is the measurement of the electric current and/or voltage in the circuit. Jones and Makin,[42] and later Makin and Lees,[43] measured the charging of solid spheres by connecting an RC circuit to the discharging electrode and recording the voltage with an oscilloscope. Comparison of this measurement technique against Faraday cup measurements revealed that this technique underrepresented the charge obtained by the spheres, although later investigations[44] suggested that this discrepancy was caused by the configuration of the sensing circuit. Tobazéon directly integrated the current to obtain the charge on a metal sphere moving between electrodes.[30] Similarly, Khayari and Peréz recorded the current pulses caused by a solid sphere charging in a leaky dielectric medium, where the sphere would charge, lift off and then fall as the charge leaked away.[45] They observed that the charge transferred during the pulse was much lower than the charge acquired by the particle as determined through a force balance approach. Knutson et al. also recorded the current for microscopic metal spheres, measuring the time-average current as a function of applied potential.[29] More

DOI: 10.1021/acs.langmuir.7b03375
Langmuir 2017, 33, 13945−13954

recently, Drews et al. estimated the charge of metal coated spheres based on the measured current and sphere velocity as the sphere crossed the centerpoint between two electrode.[28] Extending the technique of direct current measurement to liquid spheres, Im et al. used an electrometer to measure the current on a droplet shuttling charge between two electrodes, and directly integrated the current to estimate the charge on the droplet.[22]

One complication to using the current signal to extract the droplet or particle charge is the sharp increase and subsequent decay of the current each time the droplet or particle contacts the electrode. The origin of this pulse in the current is the rapid charge transfer that occurs during a brief dielectric breakdown event between the incoming droplet or particle and electrode.[24,30,32] The duration of the observed current pulse is controlled through the measuring circuit elements (i.e., the actual charge transfer between electrode and droplet may occur over a much shorter time period than the observed current pulse).[24,30,32,45] Previous efforts to extract the particle or droplet charge from the current signal have ignored this pulse, either through time averaging the signal,[29] only using portions of the signal far away from the pulse,[28] or integrating the entire signal,[22,30] all of which may inaccurately estimate the amount of charge acquired by the droplet.

In this work, we develop and validate an amperometric methodology for measuring the charge acquired by a droplet, without relying on visual observations of the droplet velocity. Specifically, we present a model for the observed current using the superposition of the natural response of an RLC circuit and an induced current caused by the droplet motion, as described by the Shockley–Ramo theorem.[46,47] By performing a nonlinear regression of the experimental data to the theoretical model we are able to extract the charge on the droplet. We then simplify the model to eliminate the need for visual observation of the droplet and compare the charge obtained through this method to the force balance charge estimates to find a strong linear correlation between the techniques. Finally, we use our direct measurement technique to probe charge transfer into droplets as a function of applied potential and compare our charge measurements to the limiting theoretical charge as derived by Maxwell.[31]

EXPERIMENTAL APPARATUS

The experimental apparatus is sketched in Figure 1 top, and is similar to that used in previous investigations.[24] Thin film gold electrodes 1 mm wide and 20 mm long were deposited on glass substrates using standard photolithography techniques (see Figure S1 for details of the electrodes). Two of these electrodes were placed in a polystyrene cuvette with a nonconductive spacer at the top and bottom, and the cuvette was filled with 100 cSt silicone oil, a transparent nonconductive oil. One electrode was connected to a high-voltage power supply (Trek model 610E), while the other was connected through an electrometer (Keithley 6514) to ground. The analog signal from the electrometer was recorded using a data acquisition card (National Instruments USB-6251) at a sampling frequency of 50 kHz; this high frequency is necessary to obtain adequate time resolution of the current. Video was taken at a frame rate of 500 frames per second using a Phantom v7.3 camera. Simultaneous video and current measurements were taken and postprocessed in Matlab to correct for slight differences in the timing. It is important to note that the currents observed here are small (on the order of nA), and as such proper care must be

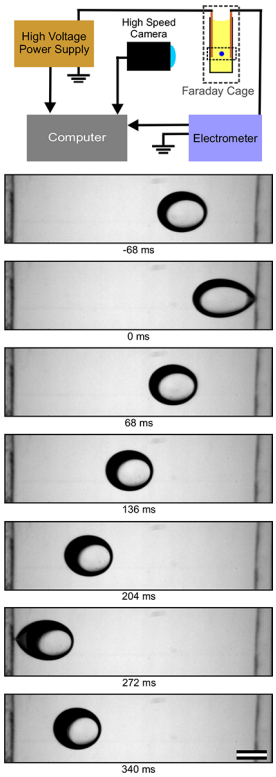

Figure 1. Top: Schematic of experimental setup. An electrometer records the instantaneous current while a high speed camera captures droplet motion. Bottom: Representative time lapse images of a 2 μL water droplet bouncing between electrodes in 100 cSt silicone oil in 438 V/mm electric field. The charged droplet initially moves to the right, where it contacts an electrode and acquires a charge of the opposite sign. The droplet then moves left until it contacts the left electrode and the process repeats. Scale bar is 1 mm. See also the Supplementary Movie.

taken to correctly shield the equipment from electrical noise. Accordingly, the experimental cell was encased in an aluminum Faraday cage with holes strategically placed to allow visualization of the experimental cell with the camera. In the absence of a droplet, the baseline current was approximately 77 ± 10 pA and invariant in time. This baseline current is possibly caused by leakage current through the electrical connections or trace impurities in the oil phase. To minimize the contribution associated with the baseline current, we measured the baseline current just prior to introducing a droplet to the cell, and subtracted the average value from the final current trace.

Figure 1, bottom shows a representative time-lapse sequence of images from a video of a 2 μL deionized water droplet oscillating between two electrodes (see also the Supplementary Movie). The droplet, initially negatively charged, moves right and makes contact with the powered electrode and acquires a net positive charge. The droplet then moves left to the ground electrode, acquires net negative charge, and moves toward the right electrode, where the process repeats indefinitely until the electric field is turned off. Similar bouncing behavior has been widely reported in previous work;[5,14,18,22−27] the main goal here is to elucidate the current signal in the context of the discrete charge transfer events at each bounce.

DOI: 10.1021/acs.langmuir.7b03375
Langmuir 2017, 33, 13945−13954

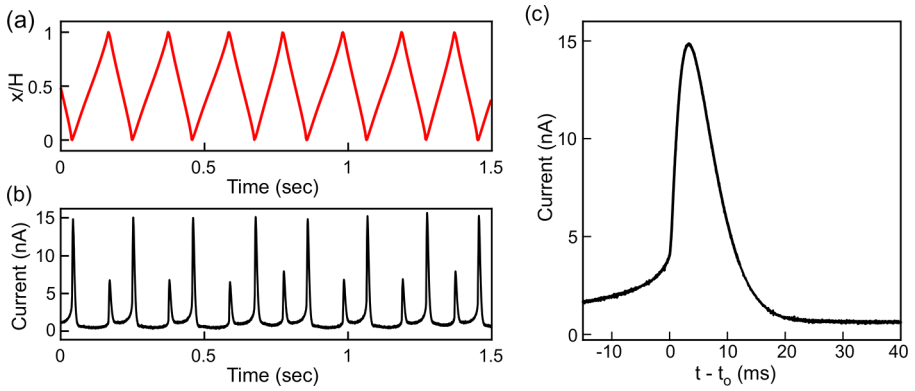

Figure 2. Representative droplet trajectory and simultaneous current. (a) Representative trajectory of a 2 μL water droplet "bouncing" between electrodes in a 500 V/mm electric field. The droplet centroid position, x, is normalized by the electrode separation distance. The positive electrode is at $x/H = 1$; the negative electrode at $x/H = 0$. (b) Simultaneous current measurements. Note that the current is low except when pulses occur when the droplet contacts the electrode. (c) Magnified view of the first peak in (b).

INTERPRETATION OF THE CURRENT

Representative plots of the droplet position (Figure 2a) and instantaneous current (Figure 2b) versus time reveal that large spikes in current occur each time the droplet reverses direction. In other words, charge transfer during each "bounce" causes a distinct pulse in the current. Note that the current in the system appears relatively steady and low, except when the droplet makes contact with the electrodes. Also note the magnitude of the droplet velocity is much greater after contact with the positive electrode (when the droplet is moving left, or down on the plot). The baseline current is also greater during this time, as can be seen in Figure 2b.

Zooming in on one such pulse (Figure 2c), we see that even before the droplet makes contact with the electrode the current gradually increases. The droplet then makes contact at $t = t_0$, and the current rapidly increases. The time of contact, t_0, is found by numerically differentiating the current data to find the time at which the change in the current increases most sharply, i.e., when d^2i/dt^2 is maximum. Following contact, we see a sharp increase (over approximately 2 ms) in the magnitude of the current to roughly 13 nA followed by a gradual decay over 15 ms to a steady value. High speed video at the point of contact (not shown) indicates that the droplet remains in contact with the electrode for approximately 250 μs, a much shorter time scale than the decay time of the pulse. This observation, combined with previous observations of short duration flashes of light,[24] strongly indicates that the circuitry, rather than the physical charge transfer dynamics at the water-electrode interface, is what governs the dynamics of the current response.

To test this idea, and to gain insight into the shape of the current pulse, we applied a step change to the applied potential in an experimental cell without any droplet present. Figure 3 shows the resulting "natural" response of the experimental circuit to a step change of 2800 V. Note that a current pulse occurs simultaneously with the step change in the voltage; this pulse has the same qualitative shape as the pulse which occurs when a droplet makes contact with an electrode, except that in Figure 3 there is no increase in the current prior to the voltage change. The time scale over which the pulse decays (20 ms) is qualitatively similar to the case when a droplet charges, and was observed in other trials to be independent of the magnitude of the potential step change. These observations strongly

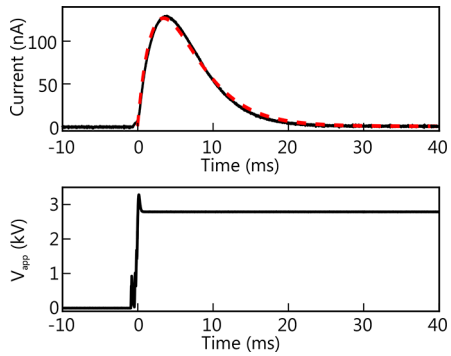

Figure 3. Current response to voltage step. The natural current response to a step change in the applied voltage in the experimental cell, without an droplet. At $t = 0$, the applied voltage (bottom) is stepped from 0 to 2.8 kV. The current (top, in black) is seen to increase initially and decrease in response to the step change. The red dashed line (top) is eq 4 fit via nonlinear regression.

corroborate the notion that the shape of the current pulse is controlled by the circuit elements.

The experimental circuit can be thought of as having a resistor (connections and the electrometer) in series with a capacitor (experimental cell, with the two metal electrodes holding charge and the nonconductive oil acting as the dielectric). The observed current response to the voltage step change is not simply an RC response, however, since the natural response of an RC circuit has a discontinuity at the peak maximum.[48] Instead, here we see a rapid increase then a more gradual decay; in other words, the current pulse in Figure 3 has the shape of the natural response of a series resistor-inductor-capacitor (RLC) circuit.[48] The high-voltage power supply presumably provides the inductance in the circuit, as inductive filters are commonly used to reduce the ripple current in rectifiers.[49] The current response of a series RLC circuit to a step change in the voltage is[48]

$$i_{\text{pulse}}(t) = \frac{V_0}{L}\left(\frac{\exp(s_1 t) - \exp(s_2 t)}{s_2 - s_1}\right) \quad (4)$$

where V_0 is the initial capacitor voltage, L the inductance of the system, and $s_{1,2}$ are characteristic frequencies determined by the resistance R and the capacitance C as follows:

DOI: 10.1021/acs.langmuir.7b03375
Langmuir 2017, 33, 13945−13954

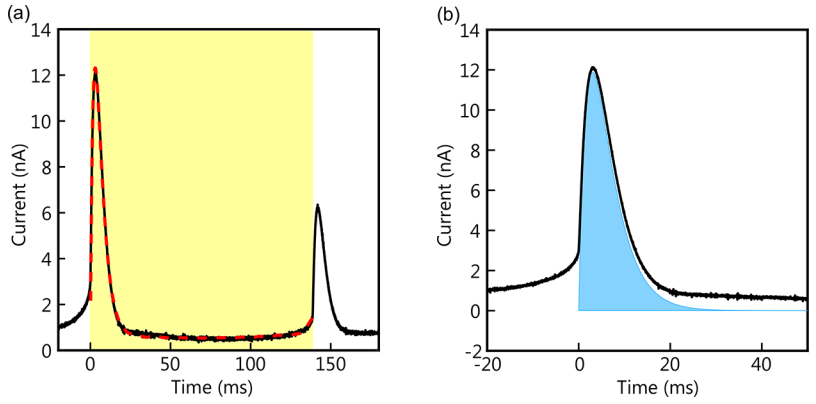

Figure 4. (a) Representative current race (black) showing two bouncing pulses for a 2.0 μL deionized water droplet (E = 438 kV/mm). The red dashed line is eq 9, using parameters fit via nonlinear regression. The shaded region (yellow) indicates the region over which eq 9 pertains. (b) Magnified view of the first pulse in (a), illustrating the integrated "natural" (RLC) contribution to the total current as the (blue) shaded region. The best fit parameters for eq 9 (red dashed line) were substituted into eq 4 to obtain the blue shaded region.

$$s_{1,2} = -\frac{R}{2L} \pm \sqrt{\left(\frac{R}{2L}\right)^2 - \frac{1}{LC}} \tag{5}$$

As shown in Figure 3, the current predicted by eq 4 fits the observed current pulse extremely well for appropriate values of R, L, and C. For the current data shown in Figure 3, the best fit values of s_1 and s_2 were −289 Hz and −290 Hz, respectively. Both frequencies were real, consistent with an "over damped" response that is desirable for high voltage power supplies.

Because of the similarity in shape between the current pulse due to droplet charging and the natural response of the RLC circuit, it is tempting to assume that the pulse in Figure 2c is entirely due to a step change in potential during the droplet charge transfer. Note, however, that there is a crucial qualitative difference between the shapes of the pulses in Figures 2c and 3. Specifically, there is a significant rise in the current magnitude just prior to the droplet making contact with an electrode, as well as an overall increase in the baseline current when the droplet moves from the positive to negative electrode (see Figure 2b). It is well-known that a charge moving toward an electrode induces an "image" charge that also moves, generating an "induced current." We hypothesize that the motion of the charged droplet between the electrodes induces a current through the system. The classic Shockley−Ramo theory[46,47,50] describes the current produced by a particle with charge Q moving with velocity $\vec{u}$ toward a perfectly conducting electrode as

$$i_{\text{induced}} = Q\vec{u}\,\frac{dE}{dV} \tag{6}$$

Here dE/dV describes the change in the electric field E, in the absence of the charged particle, as the voltage V of the electrode is changed. In our experimental geometry, the electric field between the two planar electrodes can be approximated as $E = V/H$, where H is the distance separating the electrodes. Thus, for this system, eq 6 can be written as

$$i_{\text{induced}} = \frac{Q\vec{u}}{H} \tag{7}$$

Taking into account the current pulse as well as the induced current, the total observed current is

$$i_{\text{obs}} = i_{\text{pulse}} + i_{\text{induced}} \tag{8}$$

yielding

$$i_{\text{obs}} = \frac{V_0}{L}\left(\frac{\exp(s_1 t) - \exp(s_2 t)}{s_2 - s_1}\right) + \frac{Q\vec{u}}{H} \tag{9}$$

Note that this expression pertains to the time period following contact at one electrode until contact with the opposite electrode, indicated by the shaded region of Figure 4a.[51]

There are some limitations to the Shockley−Ramo theory utilized here. First, the theory describes the current induced in electrodes by a point charge, and thus will not capture higher moments of charge present in larger (polarizable) objects. The theory will become less valid as the droplet size increases, since the theory only considers contributions from the first moment. In our experiments, the droplet radius is approximately 0.75 mm, much smaller than the 8 mm electrode separation distance (i.e., $a \ll H$). Second, we emphasize that eq 7 is specific for charges moving between parallel plate electrodes, although the use of Shockley−Ramo theory is appropriate for any electrode geometry. More complicated geometries will require knowledge of $\frac{dE}{dV}$ for use in eq 6.

The primary goal of this work is to determine the charge transferred to the droplet. We emphasize that simply integrating the observed current would yield an erroneous overestimate of the charge because of the contributions of the pulse current (i_{pulse}), whose magnitude and duration is largely determined through circuit elements. The droplet velocity $\vec{u}$ and electrode separation H are known experimentally, so a nonlinear regression is used to fit the experimentally observed current trace to eq 9 and find V_0/L, s_1, s_2, and Q.

A representative example fit is shown in Figure 4a as the red dashed line, where we see good agreement between the model and the observed current. Importantly, we find that the average best fit values of s_1 were −296.3 ± 16 and −285.3 ± 31 Hz for pulses on the positive and negative electrode, respectively, while the best fit values of s_2 were −296.1 ± 14 Hz for positive electrode pulses and −279.8 ± 23 Hz for negative electrode pulses. Note that these values for s_1 and s_2 are similar in magnitude to those calculated for the natural RLC response (cf. Figure 3). No dependence of s_1 and s_2 on the applied voltage was observed.

The model has four fitting parameters, V_0/L, s_1, s_2, and Q, two of which, s_1 and s_2, are primarily responsible for the shape of the current pulse. The duration of the current pulse (~15

DOI: 10.1021/acs.langmuir.7b03375
Langmuir 2017, 33, 13945−13954

ms) is much shorter than the droplet transit time (~150 ms) so these parameters have little effect on extracted charge; that is, the droplet charge is found through regression of the entire droplet transit not just the short duration of the current pulse. Accordingly, we have simplified the regression model by substituting the average value for s_1 and s_2 determined from experiments where a large step change in the applied voltage of the system was applied (cf. Figure 3) instead of regressing to find s_1 and s_2 for each droplet bounce.

Furthermore, we have eliminated the required visual observation of the droplet to determine its velocity by substituting the observed droplet velocity $\vec{u}$ with an average droplet velocity $\vec{u}_{avg}$ obtained from

$$\vec{u}_{avg} = \frac{H - 2a}{\Delta t} \tag{10}$$

where H is the distance between the electrodes, a is the droplet radius, and Δt is the time between subsequent current pulses. Equation 10 is the distance traveled by the droplet between electrodes divided by the travel time, or the average velocity of the droplet. The final simplified model is given as

$$i_{obs} = \frac{V_0}{L}\left(\frac{\exp(s_{1_{avg}} t) - \exp(s_{2_{avg}} t)}{s_{2_{avg}} - s_{1_{avg}}}\right) + \frac{Q\vec{u}_{avg}}{H} \tag{11}$$

where $s_{1_{avg}}$ and $s_{2_{avg}}$ are the average value of s_1 and s_2 determined from experiments where a large step change in the applied voltage of the system was applied. The droplet radius is the only required visual observation necessary to perform the nonlinear regression of eq 11 to find the droplet charge.

Figure 5 compares the droplet charge extracted from full nonlinear regression model (eq 9) to the charge extracted from a simplified regression model (eq 11). There is close agreement between the charges extracted from the simplified model and the charges extracted using the full model regression; on average the extracted charges are within 4% of each other. The method outlined here thus provides a way to extract the droplet charge without visual observation of the droplet velocity.

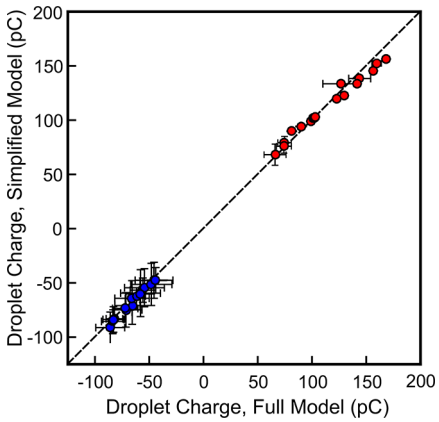

Figure 5. Comparison between droplet charge as determined using the full model (eq 9) and the simplified model (eq 11). The dashed line has a slope of one. Red markers are positive charge, and blue markers are negative charge. Each marker is the average of one experimental trial, approximately 50−200 bounces. Error bars represent one standard deviation.

As a final consistency check, we examined whether the charges determined via nonlinear regression to the current signal were correlated with charges calculated via the force balance approach. Figure 6 compares the droplet charge as estimated by the standard force balance (eq 2) to the charge measured via nonlinear regression. We assumed Hadamard-Rybczynski drag for the droplet (i.e., $\lambda = 1$). As shown in Figure 6, there is a strong linear correlation between the two measurement techniques; in other words, when the nonlinear regression technique yielded a smaller (larger) charge, the droplet was also observed to move more slowly (quickly). The ratio in charge measured between the two approaches was on average 0.957, i.e., on average a 4.3% difference, although some positive charges had disparities as large as 30% (cf. red points in Figure 6).

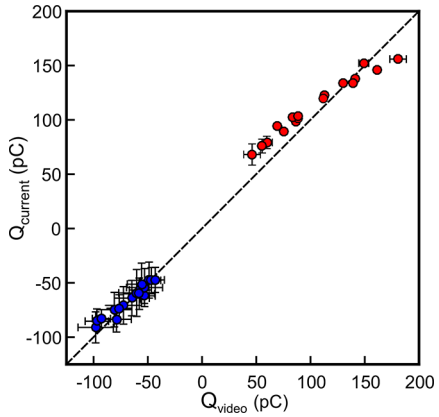

Figure 6. Comparison of the droplet charge as estimated via the force balance (eq 2) and current regression (eq 11). The dashed line has a slope of one. Red markers are positive charge, and blue markers are negative charge. Each marker is the average of one experimental trial, approximately 50−200 bounces. Error bars represent one standard deviation.

EFFECT OF APPLIED POTENTIAL

We next used the current regression technique to investigate the effect of the applied electric potential on the charge acquired by deionized water droplets. Each point in Figure 7a represents the average and standard deviation of an experimental trial, approximately 50−200 bounces (with a lower number of bounces at lower field strengths). The square points represent the charge as estimated by eq 2 using a force balance, while the circles represent the charge for the same experiments as determined from the nonlinear regression of eq 11. Red and blue refer to charging at the positive and negative electrode, respectively. Note that the magnitude of both the positive and negative charge, as measured by either the force balance or chronocoulometric fitting technique, increase linearly with the applied electric field from approximately 50 to 160 pC and from −40 to −90 pC for positive and negative charges, respectively. For the droplets considered, the distribution of charge acquired is similar for both methods. At any particular applied potential, there is little variation in positive charge acquired; the standard deviation is on average 4.6% of the mean value when determined through the force balance approach or 3.7% when determined via nonlinear regression. In contrast, the negative charge acquired at any particular potential varies significantly more, with the average standard deviation of approximately 20% and 23% of the mean

DOI: 10.1021/acs.langmuir.7b03375
Langmuir 2017, 33, 13945−13954

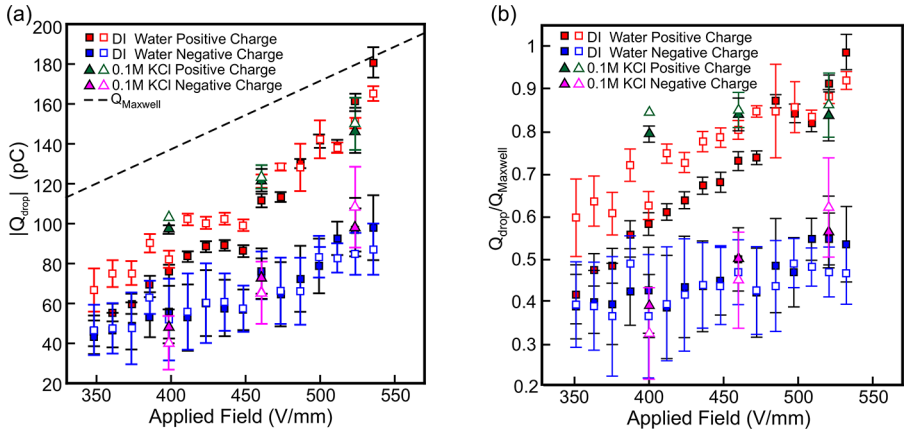

Figure 7. Effect of applied voltage on droplet charge. (a) Absolute charge acquired by the droplet vs the applied electric field. Solid markers indicate charges acquired by the droplet as calculated via the force balance method (eq 2). Open markers indicate charges obtained via nonlinear regression of the observed current (eq 11). The red and blue markers represent positive and negative charges, respectively, for DI water droplets. Green and magenta markers indicate positive and negative charges, respectively, obtained for 0.1 M KCl droplets. The dashed line represents the theoretical maximum charge as calculated by Maxwell (eq 12). (b) Absolute droplet charge normalized by the theoretical maximum charge (eq 12) vs applied electric field. For both plots, each marker is the average of one experimental trial, approximately 50−200 bounces. Error bars represent one standard deviation.

value for the force balance and nonlinear regression approaches, respectively.

To put these measurements in to context, it is useful to compare the charges to the asymptotically limiting case of charge transferred to a perfectly conducting sphere from a perfectly conducting plane,[31] namely,

$$Q_{\mathrm{Maxwell}} = \frac{2}{3}\pi^3 \epsilon\epsilon_0 a^2 E \tag{12}$$

Water droplets have finite conductivity and deform as they approach electrodes so direct comparison of the droplet charge to eq 12 should not be done. Nonetheless, eq 12 provides a useful limiting case for comparison of droplet charge across many different applied electric field strengths. The dashed line in Figure 7a indicates the value of Q_{Maxwell} as calculated above. The same trends observed in Figure 7a are presented in a different fashion in Figure 7b, which shows the ratio of the observed charge normalized on the limiting Maxwell charge. It is clear from both methods that the water droplet systematically acquires less charge than the Maxwell prediction. This result is consistent with other reports of water droplets[14,22−27] and other charged particles[28,30] receiving less charge than predicted. While it is unclear why this occurs, one possibility is that the deformation of the poorly conducting water droplet near the electrode to form a Taylor cone may limit the charge transfer, as the Maxwell prediction is based on a perfectly conducting rigid sphere.

A final key observation is that, regardless of the measurement technique, it is clear the droplet systematically acquires more charge from the positive electrode than the negative electrode. The overall disparity between the positive and negative charge is larger when estimated by nonlinear regression, although both techniques show on average a 69% increase in the positive charge compared to the negative charge. These results suggest that the charge difference is real and not the result of an incomplete force balance being used to determine the charge on the droplet.

One possible explanation for the charge disparity is the large difference in the ionic mobility between H^+ and OH^- ions. Greater insight into this hypothesis is gained by examining the four separate time scales involved in droplet charging and transit: the droplet transit time, the droplet charging time, the charge relaxation time, and ionic transport time. The droplet transit time t_{transit} is defined as the time required for the droplet to transit between the electrodes; it is experimentally observed to be on the order of 100 ms at the highest applied voltages used in these experiments (cf. Figure 3a). The droplet charging time t_{charging} is defined as the time during which charge is exchanged between the electrode and the droplet. To obtain a conservative overestimate, we approximate t_{charging} as the time in which the droplet is in apparent contact with the electrode as determined through high speed video, or at most 250 μs. The charge relaxation time is the characteristic time over which charge relaxes from the droplet surface into the droplet, defined as $t_{relax} = \epsilon\epsilon_0/\sigma$, where $\epsilon\epsilon_0$ is the droplet permittivity and σ is the droplet conductivity. For deionized water droplets t_{relax} is 7 μs. Finally, the ionic transport time t_{ion} is the time required for ions to electrophoretically move across the charge polarization layer (the Debye layer), defined as $t_{\mathrm{ion}} = \frac{\lambda_D}{\mu_e E_d}$ where λ_D is the Debye length, μ_e is the electrophoretic mobility of the charge carrier, and E_d is the electric field inside the droplet.[52] The electric field in the drop is estimated by $E_d = \frac{3}{\epsilon+2}E$, where ϵ is the dielectric constant of the droplet and E is the applied electric field.[53] Note that this is an underestimate of the actual field acting on the ions in the drop since it neglects electric field effects created from the droplet surface charge. The Debye length ($\lambda_D \sim 100$ nm) is the characteristic length over which ions must move from the droplet surface to the droplet bulk. The electrophoretic mobility of the H^+ is nearly double that of the OH^- ion (μ_e = 0.37 and 0.21 mm^2/(V s) respectively);[54] thus, t_{ion} is 25 μs for negatively charged drops and 15 μs for positively charged drops.

To recapitulate, the droplet transit time is 4 orders of magnitude larger than any of the other characteristic time scales ($t_{\mathrm{transit}} \gg t_{relax}, t_{\mathrm{ion}}$) indicating that both OH^- and H^+ ions have sufficient time to equilibrate during each droplet transit. Similarly, t_{charging} is up to 2 orders of magnitude larger than the ionic transport and charge relaxation times, suggesting that ions have sufficient time to move into the droplet while the

DOI: 10.1021/acs.langmuir.7b03375
Langmuir 2017, 33, 13945−13954

droplet remains in apparent contact with the electrode. Given these scaling estimates, it is difficult to explain the observed charge asymmetry in terms of differences in charge distributions due to differences in ionic mobility.

To further investigate the effect of charge carrier mobility on droplet charge, we performed additional experiments with aqueous 0.1 M KCl droplets moving between electrodes in a range of applied electric fields. Droplets of both conductivities received comparable amounts of charge across a variety of applied electric field strength (see Figure 7), despite the fact that the 0.1 M KCl drops have a conductivity 4 orders of magnitude larger than deionized water droplets (11 mS/cm and 0.001 mS/cm respectively). Increasing the droplet conductivity decreases both t_{relax} and t_{ion}, meaning that charge transport into the droplet during charge transfer and droplet transit is faster. Taken together with the scaling results above, the experimental results strongly suggest that some mechanism other than difference in ionic mobility is responsible for the droplet charging behavior.

An alternative explanation for the charge asymmetry might involve physical deformations to the electrode during the charge transfer event. We previously reported that high conductivity droplets create small pit-like craters at the point of near contact on the electrode.[24] Here in contrast we primarily focused on lower conductivity deionized water droplets, similar to droplets used in many other previous studies (cf. Table 1).[22,23,26,27] We examined our electrodes after deionized water droplets were bounced on them and found no evidence of changes to the electrode. Optical and scanning electron microscopy examination of the electrodes (using the same techniques as discussed by Elton et al.[24]) revealed no discernible changes. The lack of morphological changes to the electrode for deionized water droplets suggests that the charge transfer mechanism is more complex than previously thought; it is unclear how droplets that are 4 orders of magnitude different in conductivity can acquire very similar charges, yet induce markedly different physical changes to the electrode. Further studies are needed to elucidate the charge transfer mechanism at each electrode and provide more insight into the observed charge difference.

SUMMARY AND CONCLUSIONS

In this work, we presented a method by which one can measure the charge transferred to a droplet by performing a nonlinear regression to the observed current. Provided the voltage dependence of the electric field is known one can separate the contributions of the natural RLC response current and the induced current to the total current and extract the desired charge. We used the current-regression technique to probe the effect of the applied electric potential on charging of water droplets, and found that the positive charge was on average 69% greater than the negative charge. This indicates that the difference in charge acquired in not due to an incomplete force balance being used to determine droplet charge. Further work is necessary to elucidate the underlying mechanisms giving rise to this large difference in positive and negative charge transfer.

Regardless of the underlying mechanism for the observed charge disparity, the techniques demonstrated here are easily generalized to estimating the charge on any charged object moving between two electrodes. Thus, the work described here has practical implications for any application where precise control or estimation of droplet or solid particle charges are desired. In particular, this work demonstrates a method for determining the charge acquired by a droplet without visual observation of droplet motion, which may be useful for lab-on-a-chip applications that currently use large microscopes to optically track droplets moving in devices.[5,16,55] A purely electrical technique for determining charge, as provided here, allows for easier miniaturization of the devices while still permitting the measurement of droplet charge. In addition, it is difficult to observe droplets and other particles in many opaque oils and other fluids,[14] a difficulty overcome by the technique presented here. Finally, it may be possible to use the single object approach described here to consider more complicated multidrop systems such as oil–water dehydrators[2,13,56] where the observed current will be the superposition of many charge transfer events. The theory presented here for a single droplet will serve as a useful limiting case for more complicated systems.

ASSOCIATED CONTENT

Supporting Information

The Supporting Information is available free of charge on the ACS Publications website at DOI: 10.1021/acs.langmuir.7b03375.

Schematic of the photomask used to pattern metallic electrodes on glass substrates; reflection microscopy image of a gold electrode on a glass substrate (PDF)

Video of a 2 μL droplet bouncing between electrodes in silicone oil (MPG)

AUTHOR INFORMATION

Corresponding Author

*E-mail: wdristenpart@ucdavis.edu.

ORCID

William D. Ristenpart: 0000-0002-4935-6310

Notes

The authors declare no competing financial interest.

ACKNOWLEDGMENTS

We thank the UC Davis Center for Nano-Micro Manufacturing for use of their equipment in electrode fabrication. We also thank the NSF Particulate and Multiphase Processes program for support (award 1707137).

REFERENCES

(1) Cottrell, F.; Wright, A. Separating mixed liquids by electric treatment. US Patent 987117, 1911.

(2) Eow, J. S.; Ghadiri, M.; Sharif, A. O.; Williams, T. J. Electrostatic enhancement of coalescence of water droplets in oil: a review of the current understanding. *Chem. Eng. J.* **2001**, *84*, 173–192.

(3) Baroud, C. N.; Gallaire, F.; Dangla, R. Dynamics of microfluidic droplets. *Lab Chip* **2010**, *10*, 2032–2045.

(4) Seemann, R.; Brinkmann, M.; Pfohl, T.; Herminghaus, S. Droplet based microfluidics. *Rep. Prog. Phys.* **2012**, *75*, 016601.

(5) Beránek, P.; Flittner, R.; Hrobař, V.; Ethgen, P.; Přibyl, M. Oscillatory motion of water droplets in kerosene above co-planar electrodes in microfluidic chips. *AIP Adv.* **2014**, *4*, 067103.

(6) Vobecká, L.; Khafizova, E.; Stragier, T.; Slouka, Z.; Přibyl, M. Electric field driven addressing of ATPS droplets in microfluidic chips. *Microfluid. Nanofluid.* **2017**, *21*, 51.

(7) Chong, Z. Z.; Tan, S. H.; Ganan-Calvo, A. M.; Tor, S. B.; Loh, N. H.; Nguyen, N.-T. Active droplet generation in microfluidics. *Lab Chip* **2016**, *16*, 35.

(8) Link, D. R.; Grasland-Mongrain, E.; Duri, A.; Sarrazin, F.; Cheng, Z. D.; Cristobal, G.; Marquez, M.; Weitz, D. A. Electric control of

droplets in microfluidic devices. *Angew. Chem., Int. Ed.* **2006**, *45*, 2556−2560.
(9) Zagnoni, M.; Le Lain, G.; Cooper, J. Electrocoalescence mechanisms of microdroplets using localized electric fields in microfluidic channels. *Langmuir* **2010**, *26*, 14443−14449.
(10) Thiam, A. R.; Bremond, N.; Bibette, J. Breaking of an emulsion under an ac electric field. *Phys. Rev. Lett.* **2009**, *102*, 188304.
(11) Gu, H.; Murade, C. U.; Duits, M. H. G.; Mugele, F. A microfluidic platform for on-demand formation and merging of microdroplets using electric control. *Biomicrofluidics* **2011**, *5*, 011101.
(12) Mochizuki, T.; Mori, Y. H.; Kaji, N. Bouncing motions of liquid drops between tilted parallel-plate electrodes. *AIChE J.* **1990**, *36*, 1039−1045.
(13) Zhang, Y.; Liu, Y.; Wang, X.; Shen, Y.; Ji, R.; Cai, B. Investigation of the charging characteristics of micrometer sized droplets based on parallel plate capacitor model. *Langmuir* **2013**, *29*, 1676−1682.
(14) Im, D. J.; Noh, J.; Moon, D.; Kang, I. S. Electrophoresis of a charged droplet in a dielectric liquid for droplet actuation. *Anal. Chem.* **2011**, *83*, 5168−5174.
(15) Clausell-Tormos, J.; Lieber, D.; Baret, J. C.; El-Harrak, A.; Miller, O. J.; Frenz, L.; Blouwolff, J.; Humphry, K. J.; Koster, S.; Duan, H.; Holtze, C.; Weitz, D. A.; Griffiths, A. D.; Merten, C. A. Droplet-based microfluidic platforms for the encapsulation and screening of mammalian cells and multicellular organisms. *Chem. Biol.* **2008**, *15*, 427−437.
(16) Im, D. J.; Jeong, S. N.; Yoo, B. S.; Kim, B.; Kim, D. P.; Jeong, W. J.; Kang, I. S. Digital microfluidic approach for efficient electroporation with high productivity: transgene expression of microalgae without cell wall removal. *Anal. Chem.* **2015**, *87*, 6592−6599.
(17) Lee, S.; Lee, S.; Hwang, H.; Hong, J.; Lee, S.; Lee, J.; Chae, Y.; Lee, T. Ultrafast single-droplet bouncing actuator with electrostatic force on superhydrophobic electrodes. *RSC Adv.* **2016**, *6*, 66729−66737.
(18) Ristenpart, W. D.; Bird, J. C.; Belmonte, A.; Dollar, F.; Stone, H. A. Non-coalescence of oppositely charged drops. *Nature* **2009**, *461*, 377−380.
(19) Hamlin, B. S.; Creasey, J. C.; Ristenpart, W. D. Electrically tunable partial coalescence of oppositely charged drops. *Phys. Rev. Lett.* **2012**, *109*, 094501.
(20) Taylor, G. I. Disintegration of water drops in an electric field. *Proc. R. Soc. London, Ser. A* **1964**, *280*, 383−397.
(21) Fernandez de la Mora, J. The fluid dynamics of Taylor cones. *Annu. Rev. Fluid Mech.* **2007**, *39*, 217−243.
(22) Im, D. J.; Ahn, M. M.; Yoo, B. S.; Moon, D.; Lee, D. W.; Kang, I. S. Discrete electrostatic charge transfer by the electrophoresis of a charged droplet in a dielectric liquid. *Langmuir* **2012**, *28*, 11656−11661.
(23) Jung, Y. M.; Oh, H. C.; Kang, I. S. Electrical charging of a conducting water droplet in a dielectric fluid on the electrode surface. *J. Colloid Interface Sci.* **2008**, *322*, 617−623.
(24) Elton, E. S.; Rosenberg, E. R.; Ristenpart, W. D. Crater formation on electrodes during charge transfer with aqueous droplets or solid particles. *Phys. Rev. Lett.* **2017**, *119*, 094502.
(25) Eow, J. S.; Ghadiri, M. Motion, deformation and break-up of aqueous drops in oils under high electric field strengths. *Chem. Eng. Process.* **2003**, *42*, 259−272.
(26) Jalaal, M.; Khorshidi, B.; Esmaeilzadeh, E. An experimental study on the motion, deformation and electrical charging of water drops falling in oil in the presence of high voltage D.C. electric field. *Exp. Therm. Fluid Sci.* **2010**, *34*, 1498−1506.
(27) Wang, X.; Liu, Y.; Zhang, Y. Velocity difference of aqueous drop bouncing between parallel electrodes. *J. Dispersion Sci. Technol.* **2015**, *36*, 893−897.
(28) Drews, A. M.; Cartier, C. A.; Bishop, K. J. M. Contact charge electrophoresis: Experiment and theory. *Langmuir* **2015**, *31*, 3808−3814.
(29) Knutson, C. R.; Edmond, K. V.; Tuominen, M. T.; Dinsmore, A. D. Shuttling of charge by a metallic sphere in viscous oil. *J. Appl. Phys.* **2007**, *101*, 013706.
(30) Tobazéon, R. Electrohydrodynamic behaviour of single spherical or cylindrical conducting particles in an insulating liquid subjected to a uniform DC field. *J. Phys. D: Appl. Phys.* **1996**, *29*, 2595−2608.
(31) Maxwell, J. C. *A Treatise on Electricity and Magnetism*; Cambridge University Press, 2010; Vol. *1*; §175.
(32) Eslami, G.; Esmaeilzadeh, E.; Pérez, A. T. Modeling of conductive particle motion in viscous medium affected by an electric field considering particle-electrode interactions and microdischarge phenomenon. *Phys. Fluids* **2016**, *28*, 107102.
(33) Millikan, R. A. On the elementary electrical charge and the Avogadro constant. *Phys. Rev.* **1913**, *2*, 109−143.
(34) Hadamard, J. S. Mouvement permanent lent d'une sphere liquide et visqueuse dans un liquide visqueux. *CR Acad. Sci.* **1911**, *152*, 1735−1743.
(35) Rybczynski, W. Über die fortschreitende bewegung einer flssigen kugel in einem zhen medium. *Bull. Acad. Sci. Cracovi, A* **1911**, 40−46.
(36) Clift, R.; Grace, J.; Weber, M. *Bubbles, Drops, and Particles*; Academic Press, 1978.
(37) Bond, W. N.; Newton, D. A. Bubbles, drops, and Stokes' law. (Paper 2.). *Philos. Mag.* **1928**, *5*, 794−800.
(38) Stokes, G. On the effect of the internal friction of fluids on the motion of pendulums. *Trans. Cambridge Philos. Soc.* **1851**, *9*, 8−106.
(39) Davis, R. E.; Acrivos, A. The influence of surfactants on the creeping motion of bubbles. *Chem. Eng. Sci.* **1966**, *21*, 681−685.
(40) Hamlin, B. S.; Ristenpart, W. D. Transient reduction of the drag coefficient of charged droplets via the convective reversal of stagnant caps. *Phys. Fluids* **2012**, *24*, 012101.
(41) Happel, J.; Brenner, H. *Low Reynolds Number Hydrodynamics*; Prentice Hall International, 1973.
(42) Jones, L. A.; Makin, B. Measurement of charge transfer in a capacitive discharge. *IEEE Trans. Ind. Appl.* **1980**, *IA-16*, 76−79.
(43) Makin, B.; Lees, P. Measurement of charge transfer in electrostatic discharge. *J. Electrost.* **1981**, *10*, 333−339.
(44) Chubb, J. N.; Butterworth, G. J. Charge transfer and current flow measurements in electrostatic discharges. *J. Electrost.* **1982**, *13*, 209−214.
(45) Khayari, A.; Peréz, A. T. Charge acquired by a spherical ball bouncing on an electrode: Comparison between theory and experiment. *IEEE Trans. Dielectr. Electr. Insul.* **2002**, *9*, 589−595.
(46) Shockley, W. Currents to conductors induced by a moving point charge. *J. Appl. Phys.* **1938**, *9*, 635−636.
(47) Ramo, S. Currents induced by electron motion. *Proc. IRE* **1939**, *27*, 584−585.
(48) Nilsson, J. W. *Electric Circuits*, Fourth Edition; Addison-Wesley Publishing, **1993**.
(49) Whitaker, J. *AC Power Systems Handbook*, Third ed.; Taylor & Francis, 2009.
(50) Gunn, J. B. A General Expression for Electrostatic Induction and its Application to Semiconductor Devices. *Solid-State Electron.* **1964**, *7*, 739−742.
(51) A similar version of eq 9 was derived by Hamlin, albeit with an additional image charge term that overestimates the induced current contribution. See chapter 4 of *Electrical Control of the Charge, Motion, and Coalescence of Aqueous Droplets in Oil*. Hamlin, B. S., Ph.D. Dissertation, University of California Davis, Davis, CA, 2013.
(52) Forbes, T. P.; Levent Degertekin, F.; Fedorov, A. G. Droplet charging regimes for ultrasonic atomization of a liquid electrolyte in an external electric field. *Phys. Fluids* **2011**, *23*, 012104.
(53) Jackson, J. D. *Classical Electrodynamics*, 3rd ed.; John Wiley and Sons, Inc., 1999.
(54) Atkins, P.; de Paula, J. *Physical Chemistry*, 8th ed.; Oxford University Press, 2008.
(55) Drews, A. M.; Lee, H.-Y.; Bishop, K. J. M. Ratcheted electrophoresis for rapid particle transport. *Lab Chip* **2013**, *13*, 4295−4298.

DOI: 10.1021/acs.langmuir.7b03375
Langmuir 2017, 33, 13945−13954

(56) Drews, A. M.; Kowalik, M.; Bishop, K. J. M. Charge and force on a conductive sphere between two parallel electrodes: A Stokesian dynamics approach. *J. Appl. Phys.* **2014**, *116*, 074903.

DOI: 10.1021/acs.langmuir.7b03375
Langmuir 2017, 33, 13945−13954